EARTH SCIENCES
RESEARCH JOURNAL

Earth Sci. Res. J. Vol. 21, No. 2 (June, 2017): 59 - 65

UNIVERSIDAD NACIONAL DE COLOMBIA
SEDE BOGOTÁ
FACULTAD DE CIENCIAS
DEPARTAMENTO DE GEOCIENCIAS
RESEARCH GROUP IN GEOPHYSICS

ORE DEPOSITS

Metallogenic Dynamics Background of Ga'erqiong Cu-Au Deposit in Tibet, China

Yuan Ouyang[1, 2], Wunian Yang[*1], Hanxiao Huang[2], Hong Liu[2], Jianlong Zhang[2], Jianhua Zhang[2]

1.Key Laboratory of Geoscience Spatial Information Technology, Ministry of Land and Resources of the China, Chengdu University of Technology, Chengdu, Sichuan 610059, China
2. Chengdu Center, China Geological Survey, Chengdu 610081, China

*Email of Corresponding Author: ywn@cdut.edu.cn

ABSTRACT

The Ga'erqiong Cu-Au deposit, which sits on the north side of the Coqên-Xainzamagmatite belt, is a large-scale skarn-type deposit, whose ore body has formed in the skarn zone in the contact part of quartz diorite and marble of Duoai formation or the cracks of quartz diorite. Its mineralization is closely related to quartz diorite. And granite porphyry-related molybdenum ore still exists in its deep part. Currently, there are disputes about the metallogenic dynamics background of this deposit. From previous studies, this paper carried out zircon LA-LCPMS U-Pb dating and petrogeochemistry study for quartz diorite of Ga'erqiong Cu-Au deposit. The testing result indicates: quartz diorite and granite porphyry were formed respectively in 88±2Ma and 83±1Ma, belonging to the magmatic activity of the early stage of Upper Cretaceous; quartz diorite and granite porphyry have geochemical characteristics similar to those of island arc rock of subduction zone and geochemical indexes similar to "adakite." Combining with the regional tectonic evolution, we think that quartz diorite and granite porphyry were all formed in the extension environment after the collision of Lhasa block and Qiangtang block. Quartz diorite is the result of the migmatization of basic melt and acid melt evoked by asthenosphere material raise caused by lower crustal delamination; the formation of granite porphyry may be crust-mantle material's partial melting results due to delaminated lower crustal. Therefore, Ga'erqiongskarn-type Cu-Au deposit belongs to the metallogenic response to the collisional orogeny in the closing process of Meso-Tethys.

Keywords: Tibet; Zircon U-Pb Chronology; Geochemistry; Metallogenic Dynamics; Ga'erqiong Cu-Au Deposit

Origen de las dinámicas metalogénicas para el yacimiento de cobre y oro Ga'erqiong en Tibet, China

RESUMEN

El yacimiento de cobre y oro Ga'erqiong, que se ubica en el lado norte del cinturón Coqên-Xainzamagmatite, es un depósito tipo skarn a gran escala cuyo cuerpo mineral se formó en la zona Skarn, en la parte de contacto del cuarzo de diorita y mármol de la formación Duoai y de las grietas de cuarzo de diorita. Su mineralización está cercanamente relacionada a los cuarzos de diorita. La mena de molidbeno granítico relacionada a los pórfidos tiene presencia en estas zonas profundas. Actualmente, se presentan varias discusiones sobre el origen de las dinámicas metalogénicas de este yacimiento. Con base en trabajos previos, este estudio determinó la edad del circón uranio-plomo con la técnica LA-ICPMS y analizó la petrogeoquímica de cuarzos de diorita para el yacimiento Ga'erqiong. Los resultados del análisis indican que los cuarzos de diorita y los graníticos pórfidos se formaron en 88±2Ma y 83±1Ma, respectivamente, y pertenecen a la actividad magmática de la edad temprana del Cretácico Superior; los cuarzos de diorita y los graníticos pórfidos tienen características geoquímicas similares a aquellas de las rocas del arco insular en la zona de subducción e índice geoquímicos similares a la "adakita". En combinación con la evolución de la tectónica regional, se concluye que los cuarzos de diorita y los graníticos pórfidos se formaron en el ambiente extensivo tras la colisión de los bloques Lhasa y Qiantang. Los cuarzos de diorita son el resultado de la migmatización de fundición básica y fundición ácida suscitada por el material elevado a la astenosfera gracias a un deslaminado menor de la corteza; la formación de los graníticos pórfidos podría ser el resultado de la fundición parcial de material en el manto de la corteza debido a un deslaminado menor en la corteza. Además, el depósito Ga'erqiong corresponde a la respuesta metalogénica de la orogénesis colisional en el proceso de cierre del Mesotetis.

Palabras clave: Tibet; datación uranio-plomo; geoquímica; dinámicas metalogénicas; depósito de cobre y oro Ga'erqiong.

Record
Manuscript received: 23/05/2017
Accepted for publication: 30/06/2017

How to cite item
Ouyang, Y., Yang, W., Huang, H., Liu, H., Zhang, J., & Zhang, J. (2017). Metallogenic Dynamics Background of Ga'erqiong Cu-Au Deposit in Tibet, China. Earth Sciences Research Journal, 21(2). 59-65
doi:http://dx.doi.org/10.15446/esrj.v21n1.63002

ISSN 1794-6190 e-ISSN 2339-3459
http://dx.doi.org/10.15446/esrj.v21n2.65192

1. Introduction

Bangong Lake-Nujiang River Metallogenic belt includes not only ophiolite melange belt in suture zone but also the magmatite zone related to the tectonic evolution of Meso Tethys in the south and north side (Geng, Pan, Wang, Peng, & Zhang, 2011). The porphyry Cu-Au deposits, like Duobuza and Bolong, skarn-type Cu-Au molybdenum deposit like Galale, Tiangong Nile andBaibuta and orogenic-type Au deposits like Dazha and Shangxu discovered in recent years indicate that Bangong Lake-Nujiang River is a giant polymetallic belt mainly of copper, gold, and iron. Due to the limitation of the natural conditions of Northern Tibetan Plateau, the prospecting degree of the discovered deposit of Bangong Lake-Nujiang River metallogenic belt is relatively low in general (Chen et al., 2013; Tang et al., 2013; Huang et al., 2012; Huang et al., 2014; Liu et al., 2015). Only a few deposits reach the specific survey level and above. Hence, deepening the understanding of the geologic feature and genetic mechanism of current deposits with relatively high working level plays an important enlightening role in determining the next range of reconnaissance and summarizing the regularity of ore formation of the metallogenic belt of Bangong Lake-Nujiang River.

Ga'erqiong Cu-Au Deposit is a large-scale skarn-type Cu-Au Deposit which is located 20 km west to Gyai County, Ngari Prefecture, Tibet. Chinese deposit scientists have conducted relatively detailed studies in aspects of the geologic feature, geochemistry of mineral deposits, metallogenetic chronology and diagenetic and metallogenic geodynamics of Ga'erqiong Cu-Au Deposit (Tang et al., 2013; Yao et al., 2013; Lei et al., 2012). But consensus hasn't been reached yet about the metallogenic dynamics background of Ga'erqiong Cu-Au Deposit. Currently, there are two different viewpoints: first, the formation of Ga'erqiong Cu-Au Deposit is related to southward subduction of Bangong Lake-Nujiang River (Lei et al., 2012; Deng, Tang, Li, Yao, & Wang, 2011); and second, this deposit was formed in the extension environment after the collision of Lhasa block and Qiangtang block (Tang et al., 2013; Yao et al., 2013). Given this, by detailed field investigations and previous studies, this paper conducted an analysis of chronology and geochemistry to granide which is closely related to mineralizing relation, deeply explored the cause of formation of this ore-related intermediate-acid rock and analyzed metallogenic dynamics background of Ga'erqiong Cu-Au Deposit. Our results provide a foundation for studies of the mineralization process and metallogenic prediction of Ga'erqiong Cu-Au Deposit.

2 Metallogenic Geological Background

Bangong Lake-Nujiang River suture zone is an important tectonic line across central Qinghai-Tibet Plateau. On the south and north sides are respectively Gangdise block and Qiangtang block (Zhu et al., 2009). The suture zone is marked by interruptedly distributed ophiolite fragments, which has typical characteristics of accreting orogenic belt (Pan et al., 2007). The main body of south Qiangtang is Jurassic marine basin. Some sections of the southern rim have accreting mélange (Geng et al., 2011); Lhasa block may originate from the north side of Australia. It has a distribution pattern of the old stratum in the middle and new stratum in two sides (Zhu, Zhao, & Niu, 2001). The Precambrian crystal old base in the middle has experienced multi-phase metamorphism and presented unconformable contact with Mesozoic volcanic, sedimentary layers. Mesozoic and Cenozoic marine and interactive marine and terrestrial stratum and volcanic-sedimentary stratum are the main stratum of south and north sides (Geng et al., 2011). Under the influence of tectonic evolution of Meso and Neo-Tethys ocean, the main tectonic line of north and middle part of Lhasa block runs nearly east-west. Nearly east-west fracture apparently controlled the space distribution and form of magmatite. Large-scale island arc volcanic activities happened in intermediate and late Jurassic epoch, which belongs to a set of rock association dominated by andesite. The volcanic has geochemical characteristics of continental margin arc, whose formation is related to the south subduction of Meso-Tethys. The emplacement of intermediate-acidic rocks mainly happened during the period from Early Cretaceous Epoch to the early stage of Upper Cretaceous, with stocks and batholiths in nearly east-west zonal distribution and the rock type transforming gradually from type I granite at the initial stage to S-type granite at the later stage (Lv et al., 2011). Therefore, according to the distribution feature of magmatite, considering Shiquan River-Lhaguo Tso-Yongzhu-Namtso-Lhari fault zone as the boundary, Lhasa block can be divided into north Gangdise and middle Gangdise, while the border of middle Gangdise and the further south Gangdise arc-ridge fault-uplift zone is Ga'er-Longgeer-Zhari Namco-Cuomai fault zone (Zhu et al., 2009; Zhu et al., 2001).

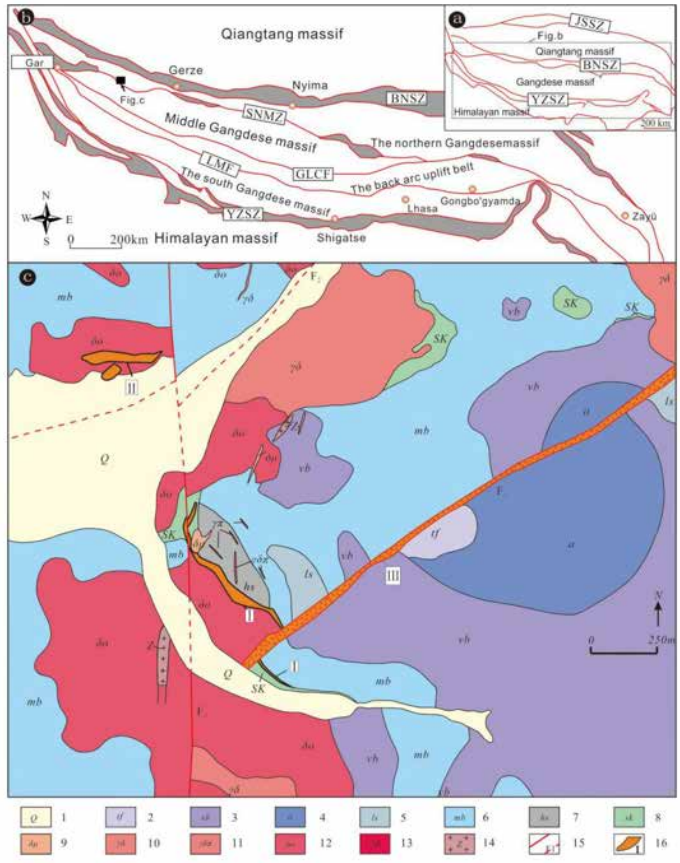

Figure 1. Schematic geological map of the Ga'erqiong Cu-Au gold deposit
1- quaternary; 2- cinerite; 3- volcanic breccia; 4- volcanic agglomerate; 5- limestone; 6- marble; 7- hornstone; 8- skarn; 9-diorite prophyrite; 10-granodiorite; 11- granodiorite porphyry; 12- quartz diorite; 13- granite porphyry; 14- pegmatite; 15- fault and inferred fault; 16- ore body

Ga'erqiong Cu-Au Deposit is tectonically located on the south rim of the west of north Gangdise (Fig. 1a), whose formation is related to limestone and marble of Early Cretaceous Epoch Duoai formation (K1d) and intermediate-acid rock of Upper Cretaceous. It belongs to typical skarn-type deposit, but porphyry-type molybdenum ore bodies exist in deep part of the reservoir (Tang et al., 2013). Intermediate-acid rock and present stratum relation of remarkable intrusive contact. Under the influence of emplacement, limestone and mud-rock of Duoai formation (K1d) are respectively marbleized and hornfelsed (Zhang et al., 2013; Li et al., 2011). Copper (gold) ore body I and II that have been found are controlled by both surrounding rock and intermediate-acid rock and are generated in the skarns near the contact zone of quartz diorites and marbles and the cracks of quartz diorite respectively. Ore body I and II are skarn-type.Metallic minerals such as chalcopyrite, bornite and native gold, etc. were generated together with quartz stockwork, which indicates that the mineralization of copper and gold mainly happened in hydrothermal mineralization period (Asis et al., 2017). Ore body III is distributed along structural fracture belt (F_1) north to east, which belongs to ore body of iron, copper and gold under control of structural fracture belt and iron-oxide copper gold (IOCG) ore body, whose formation may be related to the intrusion of aplite and granite porphyry and activities of north-east fault. Also, Skarn ore of Ga'erqiong Cu-Au Deposit contains rare intermetallic compounds of Ni-Cr-Fe and Cu-Zn (Xiao et al., 2012).

3 Sample Collection and Petrology Features

The distribution of intrusive body in Ga'erqiong Cu-Au Deposit area is relatively extensive (Fig. 1c). The intrusive body belongs to a set of intermediate-acid composite rock body, which mainly includes quartz diorite, granodiorite, quartz diorite, aplite, etc. and presents various forms such as stock, apophysis, and dike (Tang et al., 2013). The ore body has distinct characteristics of multiperiodic magmatism. The intrusive contact relationship of rock masses in the field suggests that the formation of quartz diorite and granodiorite was relatively early, while quartz diorite and aplite were formed later. Four pieces of quartz diorite and four pieces of granodiorite which are closely related to mineralization were taken as samples. The quartz diorite was taken from earth surface far away from tectonic alteration zone; the granodiorite was taken from the north of the mine. Both of them are fresh and without alteration.

Quartz diorite: It is mainly distributed in the middle and south part of the mine. There are irregularly-shaped dark inclusions in the rock. Boundaries of the listing and quartz diorite are clear with fine-grained rims and chilled borders. The rock is gray, off-white subhedral granular texture, and massive structure. It mainly consists of anorthose, hornblende, potassium feldspar, biotite, quartz and a few monoclinic pyroxenes and metallic minerals. Anorthoses are mainly andesines with medium-fine grains and subhedralclintheriform and girdle structure, and the content is about 60%. Hornblende is in the shape of short columns, which partly experienced metasomatism of biotite and chlorite and the content is about 15%. Potassium feldspar has no or rare bicrystals, and the content is about 10%. The content of quartz is about 10%, whose fine grains are in irregular shape and filled among feldspars with an uneven distribution. Biotite is about 5%. Monoclinic pyroxene is relatively less and often in irregular form or short column (Fig.2).

Granodiorite: It is light gray or off-white in fine-grained texture and massive structure. Its primary minerals are anorthose, quartz, potassium feldspar, hornblende and a few iron pyrite and biotite, which are mostly subhedralanhedral crystals with a grain size of 0.3 to 3 mm. Epidotization and chloritization can be seen in fractures. Alteration inside the rock is uneven.

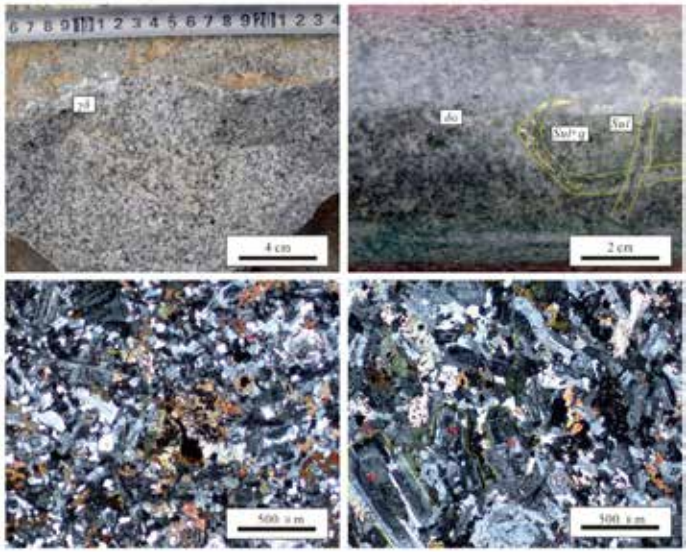

Figure 2. Field photos and micrographs of granitoid in Ga'erqiong area

4 Analysis Method and Result

4.1 Analysis Method

Analysis of major element, rare earth element, and microelement is completed in Southwest China Supervision and Inspection Center of Mineral Resourced, Ministry of Land and Resources (Chengdu Center, China Geological Survey, Chengdu Institute of Geology and Mineral Resources). According to GB/T 14506.28-93 Methods for Chemical Analysis of Silicate Rocks, the detected temperature is 18°C to 25°C, and the humidity is 35% to 65%. The major element is tested using AXIOS-X fluorescence spectrophotometer, whose analytical precision is higher than 5%; microelement is tested by ICP-MS method, using plasma mass spectrometry (X-series), whose precision is greater than 5%. The separation of zircon is finished in Lang fang Cheng xin Geo-service Co., Ltd. Backscattered electronic phase, image analysis of zircon cathodoluminescence and zircon U-Pb dating are all conducted in China University of Geosciences (Wuhan) State Key Laboratory of Geological Process and Mineral Resources (GPMR). Backscattered electronic phase and cathodoluminescence image analysis mainly aim at confirming zircon particle's internal structure, determining the test point and avoiding cracks and inclusions. Zircon U-Pb isotope in situ analysis is conducted by use of Agilent7500a inductively coupled plasma mass spectrometry of Agilent Company and GeoLas2005 excimer laser ablation on-line system of MicroLas Company (Ridzuan, Zahar, & Noor, 2017). Helium is used as a carrier gas of ablation material. The spot diameter of laser beam is 32μm. Revision is implemented with standard zircon 91500 used as the external standard and NIST610 as the internal standard. Data obtained from experiments is processed by ICPMDataCal software. After common Pb correction, isoplot 4.15 is used for the calculation of the weighted average age of zircon and the drawing of concordia diagram. For method and process, see document (Ludwig, 2013). The obtained isotope ratio and age error are on the 1σ level.

4.2 Geochemistry

For sample analysis result of quartz diorite and granodiorite, see List 1. SiO_2 content of tested granide is 53.73% to 61.58%, among which the SiO_2 content of quartz diorite sample is between 53.73% and 56.16% (averagely 55.28%) and that of granodiorite is 60.48% to 61.58% (averagely 61.16%). The Na_2O content is 0.79% to 5.19% (averagely 3.18%), the K_2O content is 2.08% to 2.92% (averagely 2.52%), and total alkali content w (Na_2O+K_2O) is 7.13% to 7.84% with an average of 7.41% which is alkali-rich. The ratio of w (Na_2O/K_2O) is between 1.56 and 2.51 with an average of 1.98%. The Rittman index (σ) is 1.80 to 4.49, which belongs to calc-alkaline rock and falls in high-K calc-alkaline series rock area in SiO_2-K_2O diagram (Fig.3a); Al_2O_3 content is between 15.10% and 17.39% with an average of 16.26%. Aluminum saturation index A/CNK is between 0.67 and 0.80 (averagely 0.76). A/NK is between 1.42 and 1.64 (averagely 1.51). In CIPW standard mineral calculation, diopside (DI) appeared, and corundum (C) didn't, which belongs to quasi-aluminous series (Fig.3b). The overall characteristics of samples suggest that granide in this area mainly belongs to quasi-aluminouscalc-alkaline granite series rock (Rahim & Usli, 2017).

Table.1 The major and trace elements characteristic values of granitoids in Ga'erqiong area

Lithology	Unit	Granodiorite				Quartz-diorite			
SiO_2	10^{-2}	60.48	61.53	61.05	61.58	53.73	56.16	55.14	56.08
Al_2O_3	10^{-2}	15.71	15.15	15.54	15.10	17.39	17.09	16.94	17.12
Fe_2O_3	10^{-2}	1.52	0.79	2.14	1.97	5.19	4.65	4.72	4.42
FeO	10^{-2}	1.97	1.94	1.79	2.18	3.37	2.64	3.11	2.90
CaO	10^{-2}	5.98	6.57	5.40	4.90	6.17	5.85	6.65	5.87
Na_2O	10^{-2}	5.22	4.70	4.87	4.68	5.04	5.04	4.55	5.02
K_2O	10^{-2}	2.08	2.65	2.26	2.72	2.11	2.63	2.92	2.82
MgO	10^{-2}	4.08	3.95	3.81	3.96	3.43	3.12	3.10	2.90
MnO	10^{-2}	0.06	0.05	0.06	0.07	0.07	0.10	0.11	0.10
P_2O_5	10^{-2}	0.24	0.22	0.25	0.23	0.41	0.38	0.39	0.39
TiO_2	10^{-2}	0.71	0.65	0.74	0.70	1.13	0.90	0.95	0.91
LOI	10^{-2}	1.64	1.50	1.82	1.58	1.44	1.04	0.94	1.01
Total	10^{-2}	99.69	99.70	99.73	99.67	99.48	99.60	99.52	99.54
w (Na_2O+K_2O)	10^{-2}	7.30	7.35	7.13	7.40	7.15	7.67	7.47	7.84
w (Na_2O/K_2O)	10^{-2}	2.51	1.77	2.15	1.72	2.39	1.92	1.56	1.78
FeOT/MgO		0.82	0.67	0.97	0.99	2.31	2.15	2.32	2.31
Mg#		0.69	0.73	0.65	0.65	0.44	0.46	0.44	0.44
A/NK		1.45	1.43	1.49	1.42	1.64	1.53	1.59	1.51
A/CNK		0.72	0.67	0.77	0.77	0.80	0.78	0.75	0.78
C	10^{-2}	0.00	0.00	0.00	0.00	0.00	0.00	0.00	0.00
Di	10^{-2}	0.68	11.91	15.14	9.08	8.56	7.68	8.40	10.86
DI	10^{-2}	72.48	64.26	64.46	65.44	66.83	56.30	60.75	57.76
σ	10^{-2}	1.80	2.97	2.85	2.74	2.88	4.49	4.32	4.43
La	10^{-6}	22.7	22.2	27.6	23.7	25.9	32.3	31.1	31.0
Ce	10^{-6}	42.6	42.1	47.9	42.5	52.2	60.3	59.3	58.1
Pr	10^{-6}	4.91	4.81	5.34	4.84	6.57	7.22	7.13	6.94
Nd	10^{-6}	18.2	18.0	19.7	17.5	27.2	28.5	28.7	27.7
Sm	10^{-6}	3.2	3.2	3.4	3.2	5.9	5.7	6.0	5.5
Eu	10^{-6}	1.07	0.94	1.08	0.95	1.74	1.60	1.67	1.54
Gd	10^{-6}	2.91	3.08	3.16	2.99	6.09	5.69	5.88	5.48
Tb	10^{-6}	0.42	0.42	0.43	0.39	0.91	0.81	0.85	0.80
Dy	10^{-6}	2.35	2.35	2.50	2.33	5.45	4.94	5.13	4.89
Ho	10^{-6}	0.44	0.46	0.49	0.43	1.07	1.02	1.03	0.95
Er	10^{-6}	1.27	1.37	1.33	1.26	3.22	3.00	3.00	2.75
Tm	10^{-6}	0.18	0.18	0.18	0.17	0.43	0.40	0.43	0.39
Yb	10^{-6}	1.15	1.16	1.18	1.13	3.00	2.78	2.82	2.56
Lu	10^{-6}	0.18	0.18	0.18	0.16	0.42	0.42	0.42	0.39
Y	10^{-6}	11.1	11.5	12.0	11.0	13.2	13.5	11.1	13.6
ΣREE (NO.Y)	10^{-6}	102	100	115	102	140	155	153	149
LREE	10^{-6}	92.7	91.3	105	92.7	120	136	134	131
HREE (NO.Y)	10^{-6}	8.90	9.20	9.45	8.86	20.6	19.1	19.6	18.2
LREE/HREE (NO.Y)		10.4	9.92	11.1	10.5	5.81	7.12	6.84	7.18
(La/Yb) N		14.2	13.7	16.8	15.0	6.19	8.33	7.91	8.69
δEu		1.07	0.91	1.00	0.94	0.89	0.86	0.86	0.85
δCe		0.99	1.00	0.97	0.97	0.98	0.97	0.98	0.97
Rb	10^{-6}	63.9	80.2	68	77.9	58.2	58.8	62.2	61.6
Ba	10^{-6}	298	326	319	352	529	529	616	575
Th	10^{-6}	5.51	6.24	6.29	5.85	6.88	8.52	8.48	8.29
U	10^{-6}	1.41	1.62	1.44	1.42	1.44	2.31	1.94	2.16
K	10^{-6}	17267	21999	18761	22580	17516	21833	24240	23410
Ta	10^{-6}	0.64	0.66	0.75	0.7	0.6	0.7	0.67	0.69
Nb	10^{-6}	10.8	10.8	12.2	11.6	10.4	10.9	11	11.4
La	10^{-6}	22.7	22.2	27.6	23.7	25.9	32.3	31.1	31
Ce	10^{-6}	42.6	42.1	47.9	42.5	52.2	60.3	59.3	58.1
Sr	10^{-6}	449	361	430	376	768	583	607	613
Nd	10^{-6}	18.2	18	19.7	17.5	27.2	28.5	28.7	27.7
P	10^{-6}	2110	1935	2198	2022	3605	3341	3429	3429
Zr	10^{-6}	123	160	157	150	147	137	151	150
Hf	10^{-6}	3.31	4.09	4	3.8	4.02	3.96	4.17	4.09
Sm	10^{-6}	3.24	3.24	3.44	3.17	5.92	5.7	5.97	5.47
Ti	10^{-6}	4255	3896	4435	4195	6772	5394	5694	5454
Yb	10^{-6}	1.15	1.16	1.18	1.13	3	2.78	2.82	2.56
Lu	10^{-6}	0.18	0.18	0.18	0.16	0.42	0.42	0.42	0.39
Nb/Ta		16.9	16.4	16.3	16.6	17.3	15.6	16.4	16.5
Zr/Hf		37.2	39.1	39.3	39.5	36.6	34.6	36.2	36.7
Rb/Sr		0.14	0.22	0.16	0.21	0.08	0.10	0.10	0.10
Rb/Ba		0.21	0.25	0.21	0.22	0.11	0.11	0.10	0.11

The total amount of rare earth element of granodiorite and quartz diorite in this area is between 100 and 155×10^{-6} with an average of 127×10^{-6}. The rare earth element content of quartz diorite is 100 to 115×10^{-6}(averagely 105×10^{-6}), which is obviously lower than that of granodiorite (ΣREE: 140~155×10^{-6}, averagely 150×10^{-6}). LERR/HERR is 5.8 to 1.1 (averagely 8.6) and $(La/Yb)_N$ is 6.2 to 16.8 (averagely 11.4), which indicates that LREE is enriched while HREE is depleted, and the fractionation is clear. δEu is averagely 0.9 without obvious anomaly. δCe is averagely 1.0, which suggests that the samples have no Ce anomaly. The distribution mode pattern of rare earth of granodiorite and quartz diorite is in mild right deviation. The differentiation of two lithologies is evident. The rare earth distribution of quartz diorite is above that of granodiorite (Fig. 4a). There is no obvious Eu anomaly. Tilt level of light rare earth's curve of all samples is higher than that of the heavy rare earth, which indicates that fractionation degree of light rare earth element is remarkably greater than that of the heavy rare earth element, reflecting the clear differentiation of light and heavy rare earth during magmatism.

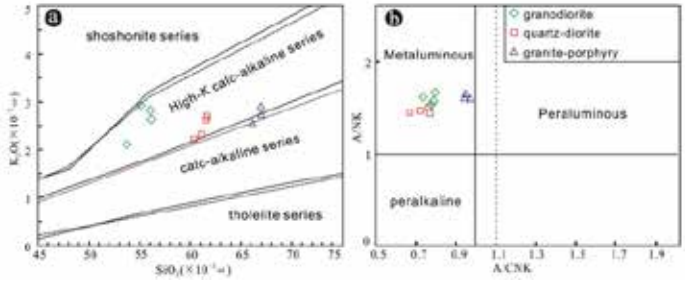

Figure 3. Diagrams of SiO_2 -K_2O and A/CNK-A/NK
(a: Base map from Pecerillo & Taylor, 1976; Middlemost, 1985; b: Base map from Maniar, & Piccoli, 1989.)

On first mantle-normalized spider diagram (Fig. 4b), the overall characteristics of granodiorite and quartz diorite of Ga'erqiong area are similar. They are both "multi-peak" fluctuant curves inclining to the right. There is an obvious differentiation between high field –strength element (HFSE) and large ion lithophile element (LILE) (Fig. 4b), which manifests as enriched in large ion lithophile element and depleted in high field -strength element, among which Ta and Nb are strongly depleted.

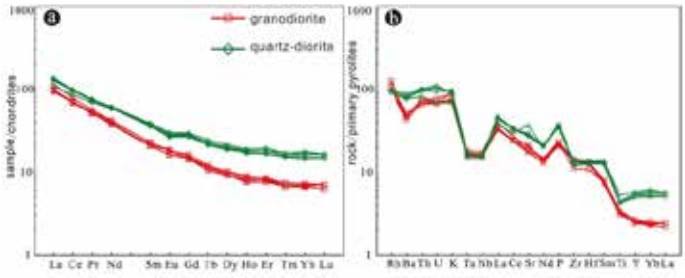

Figure 4. Chondrite-normalized REE (a) and primitive-mantle-normalized trace element patterns (b) or the magmatic rocks in Qingcaoshan region(Chonodrite values from [21]; Primitivem antle from[22])

4.3 Zircon U-Pb Age

Zircons picked from granodiorite, and quartz diorite samples of Ga'erqiong area have been tested. Check points are all in parts with clear oscillatory zoning structure. For testing position and result, see Fig. 5 and List 2. All tested zircons are transparent, colorless and with good crystalline form and typical magmatic zircon dense oscillation girdle. Zircon Th/U ratio (0.8 to 2.6) is within the magmatic zircon scope (normally metamorphic and hydrothermal origin zircon's Th/U<0.1, magmatic zircon Th/U>0.1. Zhao, 2010), which matches typical characteristics of magmatic zircon. Therefore, zircon analyzed in this paper is magmatic zircon which crystallized with Ga'erqiong granodiorite

at the same time. For young zircon, $^{206}Pb/^{238}U$ age can provide more reliable test result (Compston, Williams, & Kirschvink, 1992). The $^{206}Pb/^{238}U$ surface ages of 14 analysis points of this test are between 87 and 89 Ma, and the weighted average is 88±2Ma (MSWD=3.8) (Fig.5), which represent the crystallization age of granodiorite. The weighted average U-Pb age of granite porphyry zircon is 83±1Ma, which is about 4 Ma later than quartz diorite (Yao et al., 2012).

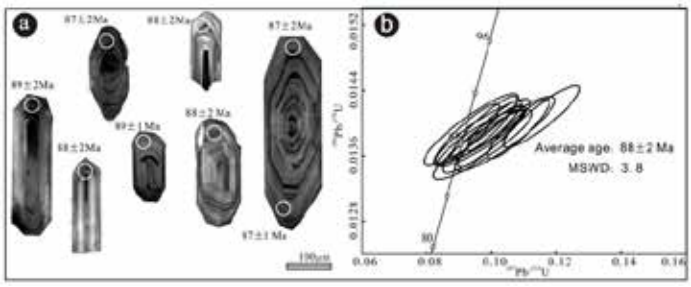

Figure 5. Cathodolum inescence (CL) images of representative zircon (a) and concordia diagrams (b) for zircons form the magmatic rocks

Table 2. LA-ICP-MS zircon U-Pb dating results in Ga'erqiong region

Number	Isotope ratios								Age (Ma)		Concordance
	$^{207}Pb/^{206}Pb$	1σ	$^{207}Pb/^{235}U$	1σ	$^{206}Pb/^{238}U$	1σ	$^{208}Pb/^{232}Th$	1σ	$^{206}Pb/^{238}U$	1σ	%
GEQ05-02	0.0611	0.0040	0.1154	0.0078	0.0141	0.0003	0.0044	0.0002	89	2	92
GEQ05-04	0.0552	0.0030	0.0974	0.0055	0.0133	0.0002	0.0041	0.0001	85	1	90
GEQ05-05	0.0514	0.0048	0.0973	0.0101	0.0137	0.0003	0.0043	0.0001	88	2	94
GEQ05-06	0.0596	0.0061	0.1161	0.0131	0.0141	0.0003	0.0044	0.0001	89	2	91
GEQ05-08	0.0488	0.0046	0.0937	0.0097	0.0139	0.0003	0.0044	0.0002	89	2	98
GEQ05-09	0.0571	0.0038	0.1022	0.0070	0.0134	0.0003	0.0044	0.0002	86	2	91
GEQ05-10	0.0535	0.0029	0.1008	0.0056	0.0140	0.0002	0.0046	0.0001	89	1	92
GEQ05-12	0.0508	0.0046	0.0974	0.0096	0.0139	0.0003	0.0044	0.0001	89	2	95
GEQ05-13	0.0562	0.0031	0.1083	0.0063	0.0139	0.0002	0.0044	0.0002	89	2	92
GEQ05-14	0.0507	0.0042	0.0965	0.0087	0.0138	0.0002	0.0044	0.0001	88	1	94
GEQ05-15	0.0576	0.0036	0.1114	0.0073	0.0144	0.0003	0.0047	0.0002	89	2	93
GEQ05-16	0.0545	0.0048	0.1042	0.0102	0.0139	0.0003	0.0043	0.0001	89	2	91
GEQ05-17	0.0513	0.0040	0.0977	0.0085	0.0138	0.0003	0.0043	0.0001	88	2	93
GEQ05-18	0.0532	0.0034	0.0997	0.0067	0.0138	0.0003	0.0046	0.0002	89	2	93

5 Results

5.1 Petrogenesis

Geochemical compositions of granitic magmas without remarkable fractional crystallization can reflect the source rock characteristics of the magma. Quartz diorite and granodiorite are both enriched in large ion lithophile elements. Compared with depleted high-field-strength elements, they show notable characteristics of depleted Nb and Ta, which is similar to that of island arc magmatite in subduction zone; both of their mineral compositions are generally consistent with those of amphibole calc-alkaline granitoid (ACG) under the mechanism of subduction (Lei et. al, 2012). In the diagram for discriminating granite Ta-Yb tectonic setting (Fig.6a), all the analyzed samples are classified into the scope of volcanic arc granite. These evidence all indicate that granite is formed in the island arc environment (Qu, Wang, Xin, H. B., Zhao, Y. Y., & Fan, 2009; You & Rahim, 2017). However, the lateral intraplate magmatism of the crust can also generate characteristics similar to those of island arc granite (Plank, 2005). Thus, only by combining the regional tectonic evolution can their tectonic settings of the formation be effectively discriminated. Current research shows that the Bangong Lake-Nujiang River section of Meso-Tethys started bidirectional subduction in Late Jurassic, and after collision and closure had occurred in middle stage of Early Cretaceous, it got into the intracontinental environment (Zhu et al., 2009; Wang, Zeng, Liu, Xiao, & Gao, 2013). The emplacement of quartz diorite and granite porphyry both happened in Late Cretaceous and notably after a collision between Lhasa plate and Qiangtang plate. This indicates that the Ga'erqiong Cu-Au Deposit is formed in Bangong Lake-Nujiang River metallogenic belt crash environment, instead of island arc environment.

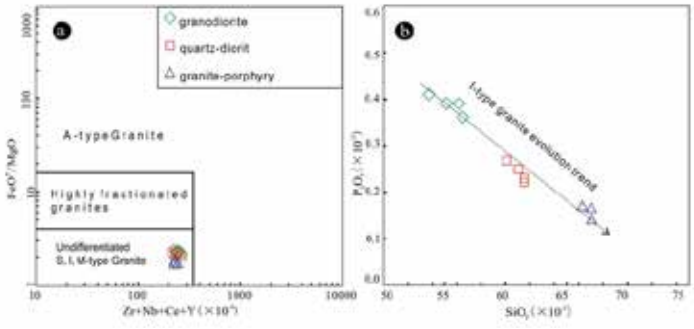

Figure 6. Tectonic environment (a) and Magma mixing trend diagrams (b) of the magmatic rocks in the Gaerqiong area
(a: Base map from [30], b: Base map from [31])

At the earliest, Adakite refers to the intermediate-acidic igneous rock with unique geochemical characteristics, which is formed by young subducting oceanic crust melting under eclogite facies condition. Its geochemical characteristics often manifest as containing $SiO_2 \geq 56\%$, high Al content ($Al_2O_3 \geq 15\%$), MgO content generally <3% (seldomly>6%), Y lower than normal island arc (generally$\leq 18\times10^{-6}$) and HREE (e.g. Yb$\leq 1.9\times10^{-6}$), Sr higher than normal island arc (seldomly$<400\times10^{-6}$), without Eu anomaly or slight negative Eu anomaly, and with low initial ratio of $^{87}Sr/^{86}Sr$ (<0.704) (Defant & Drummond, 1990). Seeing from the geochemical characteristics, quartz diorite and granodiorite both have geochemical characteristics similar to those of adakite. The research suggests that formation of adakite has various reasons including partial melting of subducted oceanic crust, crystallization differentiation of mantle-derived basaltic magma, migmatization of magma, partial melting of delaminated lower crust and partial melting of thickened lower crust. That Lhasa plate and Qiangtang plate collided in middle stage of the Early Cretaceous, which caused shortening, thickening and rapid lifting of the crust, and the low K_2O/Na_2O ratio formed by partial melting of Ga'erqiong adakite and subducted oceanic crust does not conform to reality indicates that the Ga'erqiong intermediate-acid rocks can't be formed by partial melting of subducted oceanic crust. No same-period basalt is found in the mining area. The rocks are a lack of notable negative anomaly of Sr and Eu. In the diagram for FeO^T~MgO (Fig.6a), the sample also showed no evolution tendency of crystallization differentiation (You & Rahim, 2017). All these indicate the Ga'erqiong rock is not generated from crystallization differentiation of mantle-derived basaltic magma. In addition, the Ga'erqiong adakite also can't be the result of partial melting of the thickened lower crust, as Ga'erqiong intermediate-acid and acid rocks notably contain more Mg# than melt formed by partial melting of thickened lower crust or underplating basalt. There is higher content of Cr and Ni; zirconHf isotopes of the rocks show notable characteristics of mantle-derived or mantle-crust mixed source (Yao et al., 2012). These indicate that there is mantle-derived material taking part in the diagenetic process.

Dark micro granular inclusions are generally considered as a product of halfway migmatization of mantle-derived basic magma, which is the most direct and powerful evidence for migmatization of magma. Irregular dark micro granular inclusions are found in quartz diorite. The inclusions are dioritic type with distinctive boundary with its host rock and chilled border, which indicates the inclusions are not the residual after partial melting, but the product of magma crystallization. Also, the zircon Hf isotope system has very high closure temperature which won't be changed along with partial melting or fractional crystallization. This can be used for identifying magma migmatization between different magma end members. Zircon Hf isotopes of quartz diorite have significant inhomogeneity (Yao et al., 2012), which indicates the magma source of quartz diorite has occurred magma migmatization. In the SiO2-K2O and SiO2-La second variant diagram, quartz diorite showed both good linear variation trends. All these evidence show that, during formation of quartz diorite in Ga'erqiong, the second end-member magma migmatization occurs. Therefore, quartz diorite might be formed in the post-collision extension environment after the collision of Lhasa block and Qiangtang block; lower crust delamination

caused uplifting of asthenosphere material, which further caused partial melting of lithospheric mantle and let basic melt mix with the acid melt.

Emplacement of granite porphyry is significantly later than quartz diorite, and there are no dark micro granular inclusions found in the rock, which implies that there might be different reasons for the formation of granite porphyry and quartz diorite. The granite porphyry is rich in K, which indicates it comes from thickened lower crust. The Qinghai-Tibet Plateau started crust shortening and thickening in middle stage of the Early Cretaceous. Thickening of the crust caused the formation of eclogite at the bottom of the lower crust. Due to gravity differences, the eclogite-facies lower crust is easier to have delamination; what's more, bimodal volcanic rocks appeared in Nyixung region indicates that in the early stage of Late Cretaceous, the north-central area of Lhasa block was in post-collision extension environment (Qu, Xin, Xu, Yang, & Li, 2006). Hence, partial melting of crust-mantle material caused by delamination of lower crust might be a major reason for the formation of Ga'erqiong granite porphyry.

5.2 Geodynamic background of mineralization

There are still disputes about the geodynamic mechanism of the Cretaceous volcanic rock in north and middle part of Lhasa block. So far, the mainstream opinions include: it's generated from Neo-Tethys crust's northward subduction. It's related to re-melting of thickened (delaminated) lower crust during or after collision of the Qiangtang block and Lhasa block. It's related to southwards subduction of the Meso-Tethys oceanic crust and slab breaking off (Zhu et al., 2009; Harris, Inger, & Ronghua, 1990; Coulon, Maluski, & Bollinger, 1986). In recent years, many Late Cretaceous magmatite are found in south part of the Lhasa block. These geological phenomena can't be explained by plate subduction model of the Neo-Tethys crust. Thus, quartz diorite and granite porphyry in Ga'erqiong can't be the product of Neo-Tethys crust's plate subduction. In the early stage of the Early Cretaceous, Neo-Tethys had occurred oceanic-ridge subduction (Zhu et al., 2009). Both quartz diorite and granite porphyry in Ga'erqiong have characteristics similar to those of island arc magma, and they are probably the product of Neo-Tethys' oceanic-ridge subduction. In the second place, Bangong Lake-Nujiang River Meso-Tethys had been closed at that time, and the magmatism of crust-mantle material caused by slab break-off during its southwards subduction also has the features of island arc magma. So, some scholars hold the opinion that Late Cretaceous magmatite in middle Gangdese is the common outcome of the tectonic evolution of Meso-Tethys and Neo-Tethys (Wang et al., 2013). As Ga'erqiong is about 300km away from the Yarlung-Zangbo Suture Zone, it's still lack of enough evidence so far to prove that the formation of intermediate-acid rock in Ga'erqiong is related to oceanic-ridge subduction of Neo-Tethys in early stage of Late Cretaceous. On the contrary, Ga'erqiong is not so far from the Bangong Lake-Nujiang River Suture Zone. Therefore, we think the formation of intermediate-acid rock in Ga'erqiong is more likely to be the magmatic response of Meso-Tethys' tectonic evolution.

Judging from the geologic features, the formation of ore body I and II in Ga'erqiong Cu-Au Deposit is closely related to magmatic emplacement of quartz diorite. There has been testing data to support the result of the field inspection. Zircon U-Pb age of the quartz diorite is 88±2Ma, which is consistent with the Re-Os isotope age (86.89 Ma) of molybdenite in skarn (Li et al., 2011). It indicates that 1Ma after the quartz diorite emplacement, the hydrothermal activity of magma formed the Cu, Au ore body. Zircon U-Pb age of the granite porphyry is 83±1Ma, which is significantly later than that of quartz diorite, and its mineralization is likely to be related to the subsequent mineralization of porphyry molybdenum (Yao et al., 2013). Research suggests that, the Bangong Lake-Nujiang River Meso-Tethys ocean basin opened in Late Triassic, and after ephemeral expansion, it started subduction in Late Jurassic and resulted in formation of Shiquan River – Gêrzê Subduction Zone and Rutog Subduction Zone separately in the south and north, and cultivation of abundant island arc magmatite on both sides of the suture zones at the same time (Qu et al., 2009). In the middle stage of Early Cretaceous (around 113Ma), the Lhasa block and Qiangtang block had a collision, and after that, they entered into the arc-arc (continent) collisional evolution stage. The Meso-Tethys oceanic crust subducted southwards underneath the Lhasa block. Slab break-off caused upwelling of mantle-derived material and further resulted in upwelling of mantle material, which had mantle-derived magma underplating in different scales on both sides of the suture zones (Zhu et al., 2009). After that, crust in north and middle part of Lhasa block kept thickening under the compression of north-south stress and finished shift from intracontinental compression to a partial extension in the early stage of Late Cretaceous (Rahim & Usli, 2017; You & Rahim, 2017). The thickened lower crust reached eclogite facies and started delamination, forming a series of magmation along with mineralization. It thus appears that the formation of Ga'erqiong Cu-Au Deposit is due to the metallogenic response of collision orogeny during the closing of Meso-Tethys.

6 Conclusions

(1) U-Pb age of zircon from quartz diorite that is closely related to Ga'erqiong Cu-Au Deposit and mineralization is 88±2Ma, and it's product of magmatic activity in the early stage of Late Cretaceous.

(2) Quartz diorite and granite porphyry have geochemical characteristics similar to those of island arc granitoid in a subduction zone, and they are formed in the post-collision extension environment after the collision of Lhasa block and Qiangtang block. Quartz diorite formed after asthenosphere material uplifting caused by lower crust delamination and is the mixture of basic melt formed by partial melting of lithospheric mantle and acid melt formed by partial re-melting of crustal materials. And granite porphyry is formed by partial melting of crust-mantle material caused by lower crust delamination.

(3) Formation of Ga'erqiong Cu-Au Deposit is the metallogenic response during the collision of Qiangtang block and Lhasa block.

Acknowledgements:

Wunian Yang was sponsored by the National Natural Science Funds (NO. 41071265 and NO.41372340) and the Specialized Research Fund for the Doctoral Program of Higher Education of China (NO. 20105122110006)

References:

Asis, J., Tahir, S. H., Rahim, A. R., Konjing, Z., Kob, R. C., & Tjia, H. D. (2017). Smaller benthic foraminifera Analysis of Kudat Formation, Kudat, Sabah: Preliminary Interpretation. Geological Behavior, 1(1), 27-29.

Boynton, W. V. (1984). Geochemistry of the rare earth elements: Meteorite studies. In: Henderson, P. (ed.). Rare Earth Element Geochemistry. Elsevier, 36(6), 323-338.

Chen, H. A., Zhu, X. P., Ma, D. F., Huang, H. X., Li, G. M., Li Y.B., ... Liu, C. Q. (2013). Geochronology and geochemistry of the Bolong porphyry Cu- Au deposit, Tibet and its mineralizing significance. Acta Geologica Sinica, 87(10), 1593-1611.

Compston, W., Williams, I. S., & Kirschvink, J. L. (1992). Zircon U-Pb AGES for the early cambrian time-scale. Journal of the Geological Society, 149(2), 171-184.

Coulon, C., Maluski, H., & Bollinger, C. (1986). Mesozoic and cenozoic volcanic rocks from central and southern Tibet: 39 Ar-40 Ar dating, petrological characteristics and geodynamical significance. Earth and Planetary Science Letters, 79(3), 281-302.

Defant, M. J., & Drummond, M. S. (1990). Derivation of some modern arc magmas by melting of young subducted lithosphere. Nature, 347, 662-665.

Deng, S. L., Tang, J. X., Li, Z. J., Yao, X. F., & Wang, Y. (2011). Geochemical characteristics of rock mass in the Gaerqiong Cu-Au deposit, Tibet. Journal of Chengdu University of Technology (Natural Science Edition), 38 (1), 85-91.

Geng, Q. R., Pan, G. T., Wang, L. Q., Peng, Z. M., & Zhang, Z. (2011). Tethyan evolution and metallogenic geological background of the Bangong Co-Nujiang belt and the Qiangtang massif in Tibet. Geological Bulletin of China, 30(8), 1261-1274.

Harris, N., Inger, S., & Ronghua, X. (1990). Cretaceous plutonism in Central Tibet: an example of post-collision magmatism. Journal of Volcanology and Geothermal Research, 44(1), 21-32.

Huang, H. X., Li, G. M., Liu, B., Dong, S. L., Shi, H. Z., Zhang, Z. L., & Fan, A. H. (2012). Zircon U-Pb Geochronology and Geochemistry of the Tiangongnile Skarn-type Cu-Au Deposit in Zhongba County, Tibet: Their Genetic and Tectonic Setting Significance. Acta Geoscientica Sinica, 33(4), 424-434.

Huang, H. X., Li, G. M., Liu, B., Zhang, Z. L., Ma, D., Qu, Z., Xiao, W. F., & Liu, H. (2014). Discovery of Shangxu orogenic type gold deposit in northern Tiber and its significance. Mineral Deposits, 33(3), 486-496.

Lei, C. Y., Li, Z. J., Zhang, Z., Hu, Z. H., Wang, H. X., & Song, J. L. (2012). Geochemical Characteristics and Geodynamic Significance of the Granites in the Ga'erqiong Cu-Au deposit, Tibet. Acta Geoscientica Sinica, 33(4), 601-612.

Li, Z. J., Tang, J. X., Yao, X. F., Duo, J., Liu, H. F., Deng, S. L., ... Hu, Z. H. (2011). Geological characteristics and prospecting potential of Gaerqiong copper-gold polymetallic deposit in Ali District, northern Tibet. Mineral Deposits, 30(6), 1149-1153.

Liu, H., Huang, H. X., Li, G. M., Xiao, W. F., Zhang, Z. L., Liu, B., ... Ma, D. (2015). Factor analysis in geochemical survey of the Shangxu gold deposit, northern Tibet. Geology in China, 42(4), 1126-1136.

Ludwig K. R. (2003). User's manual for Isoplot 3.00: a geochronological toolkit for Microsoft Excel. Berkeley Geochronology Center: Special Publication, 1-70.

Lv, L. N., Cui, Y. B., Song, L., Zhao, Y. Y., Qu, X. M., & Wang, J.P. (2011). Geochemical characteristics and zircon LA- ICP -MS U-Pb dating of Galae skarn gold (copper) deposit, Tibet and its significance. Earth Science Frontiers, 18 (5),224-242.

Maniar, P. D., & Piccoli, P. M. (1989). Tectonic discrimination of granitoids. Geological Society of America Bulletin Journal, 101, 635-643.

Middlemost, E. A. K. (1985). Magmas and Magmatic Rocks. London: Longman. Pag. 266.

Pan, G. T., Mo, X. X., Hou, Z. Q., Zhu, D. C., Wang, L. Q., Li, G. M., ... Liao, Z. L. (2007). Spatial-temporal framewoke of Gangdese Orogenic Belt and its evolution. Acta Petrologica Sinica, 22(3), 521-533.

Pearce, J. A., Harris, N. B. W., & Tindle, A. G. (1984). Trace element discrimination diagrams for the tectonic interpretation of granitic rocks. Journal of Petrology, 25,956-983.

Peccerillo, R., & Taylor, S. R. (1976). Geochemistry of eocene calc-alkaline volcanic rocks from the Kastamonu area, Northern Turkey. Contributions to Mineralogy and Petrology, 58, 63-81.

Plank, T. (2005). Constraints from Thorium/Lanthanum on sediment recycling at subduction zones and the evolution of the continents. Journal of Petrology, 46(5), 921-944.

Qu, X. M., Xin, H. B., Xu, W. Y., Yang, Z. S., & Li, Z. (2006). Discovery and significance of copper-bearing bimodal rock series in Coqin area of Tibet. Acta Petrologica Sinica, 22(3), 707-716.

Qu, X. M., Wang, R. J., Xin, H. B., Zhao, Y. Y., & Fan, X. T. (2009). Geochronology and geochemistry of igneous rocks related to the subduction of the Tethys oceanic plate along the Bangong Lake arc zone, the western Tibetan Plateau. Geochimica, 38(6), 523-535.

Rahim, I. A., & Usli, M. N. R. (2017). Slope stability study around kampung Kuala Abai, Kota Belud, Sabah, Malaysia. Malaysian Journal of Geoscience, 1(1), 38-42.

Ridzuan, A. A., Zahar, U. A. U., & Noor, N. A. M. (2017). Association of evacuation dimensions towards risk perception of the Malaysian students who studied at Jakarta, Medan, and Acheh in Indonesia. Malaysian Journal of Geoscience, 1(1), 07-12.

Sun, S. S., & Mchdonough, W. F. (1989). Chemical and isotopic systematics of oceanic basalts: implication for mantle composition and processes. In: Saunders, A. D. & Norry, M. J., (eds.). Magmatism in the Ocean Basins, Geological Society Special Pulication, 42, 303-345.

Tang, J. X., Zhang, Z., Li, Z. J., Sun, Y., Yao, X. F., Hu, Z. H., ... He L. (2013). The Metallogensis, Deposit Model and Prospecting Direction of the Ga'erqiong-Galale Copper-gold Ore Field, Tibet. Acta Geoscientica Sinica, 34(4),385-394.

Wang, W., Zeng, L. S., Liu, J., Xiao, P., & Gao, L. (2013). The late Cretaceous andesite Shiying and determining the geochemical characteristics in Cuoqin, Tibet. Chinese Journal of Geology, 48(2), 484-500.

Xiao, Y. F., Sun, Y., Wang, Q., Li, Z. J., Wang, Y. L., Zhang, S. M., ... He J. L. (2012). The discovery of rare intermetallic compounds (Ni-Cr-Fe, Cu-Zn) in the Garqiong copper-gold deposit of Tibet. Geology in China, 39(5), 1311-1317.

Yao, X. F., Tang, J. X., Li, Z. J., Deng, S. L., Ding, S., Hu, Z. H., & Zhang Z. (2012). Magma Origin of Two Plutons from Gaerqiong Copper-Gold Deposit and It's Geological Significance, Western Bangonghu-Nujiang Metallogenic Belt, Tibet: Implication from Hf Isotope Characteristics. Journal of Jilin University(Earth Science Edition), (S2): 188-197.

Yao, X. F., Tang, J. X., Li, Z. J., Deng, S. L., Ding, S., Hu, Z. H., & Zhang Z. (2013). The Redefinition of the Ore-forming Porphyrys Age in Ga'erqiong Skarn-type Gold—Copper Deposit, Western Bangong Lake-Nujiang River Metallogenic Belt, Xizang(Tibet). Geological Review, 59(1), 193-200.

You, L. K., & Rahim, I. A. (2017). Application of GSI system for slope stability studies on selected slopes of the crocker formation in Kota Kinabalu area, Sabah. Geological Behavior, 1(1), 10-12.

Zhang, Z., Tang, J. X., Chen, Y. C., Li, Z. J., Song, J. L., Yao, X. F., ... Wang, H. X. (2013). Skarn mineral characteristics of the Gaerqiong Cu-Au deposit in Bangong Co-Nujiang River suture zone, Tibet. Acta Petrologica Et Mineralogica, 32(3), 305-317.

Zhao, Z. H. (2010). Trace element geochemistry of accessory minerals and its applications in petrogenesis and metallogenesis. Earth Science Frontiers, 17(1), 267-286.

Zhu, D. C., Mo, X. X., Zhao, Z. D., Niu, Y. L., Pan, G. T., Wang, L. Q., & Liao Z. L. (2009). Permian and Early Cretaceous tectonomagmatism in southern Tibet and Tethyan evolution: New perspective. Earth Science Frontiers, 16(2),001-020.

Zhu, D. C., Zhao, Z. D., & Niu, Y. L. (2001). The Lhasa terrane: record of a microcontinent and its histories of drift and growth. Earth and Planetary Science Letters, 301(1), 241-255.

Zorpi, M. J., Coulon, C., & Orsini, J. B. (1991). Hybridization between felsic and mafic magmas in calc-alkaline granitoids: a case study in northern Sardinia, Italy. Chemical Geology, 92, 45-86.